# Rapid transport of large polymeric nanoparticles in fresh undiluted human mucus

Samuel K. Lai*, D. Elizabeth O'Hanlon†, Suzanne Harrold†, Stan T. Man*, Ying-Ying Wang‡, Richard Cone†, and Justin Hanes*‡§¶‖

Departments of *Chemical and Biomolecular Engineering and †Biophysics and §Institute for NanoBioTechnology, The Johns Hopkins University, 3400 North Charles Street, Baltimore, MD 21218; and Departments of ‡Biomedical Engineering and ¶Oncology, Sidney Kimmel Comprehensive Cancer Center, Johns Hopkins University School of Medicine, Baltimore, MD 21205

Edited by Alexander M. Klibanov, Massachusetts Institute of Technology, Cambridge, MA, and approved November 29, 2006 (received for review September 28, 2006)

**Nanoparticles larger than the reported mesh-pore size range (10–200 nm) in mucus have been thought to be much too large to undergo rapid diffusional transport through mucus barriers. However, large nanoparticles are preferred for higher drug encapsulation efficiency and the ability to provide sustained delivery of a wider array of drugs. We used high-speed multiple-particle tracking to quantify transport rates of individual polymeric particles of various sizes and surface chemistries in samples of fresh human cervicovaginal mucus. Both the mucin concentration and viscoelastic properties of these cervicovaginal samples are similar to those in many other human mucus secretions. Unexpectedly, we found that large nanoparticles, 500 and 200 nm in diameter, if coated with polyethylene glycol, diffused through mucus with an effective diffusion coefficient ($D_{eff}$) only 4- and 6-fold lower than that for the same particles in water (at time scale $\tau = 1$ s). In contrast, for smaller but otherwise identical 100-nm coated particles, $D_{eff}$ was 200-fold lower in mucus than in water. For uncoated particles 100–500 nm in diameter, $D_{eff}$ was 2,400- to 40,000-fold lower in mucus than in water. Much larger fractions of the 100-nm particles were immobilized or otherwise hindered by mucus than the large 200- to 500-nm particles. Thus, in contrast to the prevailing belief, these results demonstrate that large nanoparticles, if properly coated, can rapidly penetrate physiological human mucus, and they offer the prospect that large nanoparticles can be used for mucosal drug delivery.**

drug delivery | mucosal tissues | particle tracking | PEG

Treatments for cervicovaginal (CV) tract diseases, often based on drugs delivered to the systemic circulation by pills or injections, typically suffer from low efficacy (1, 2). For example, systemic chemotherapy is typically the last or strictly concurrent option, after surgery and radiotherapy, for treatment of cervical cancer (3, 4). In addition, systemic medications can lead to significant adverse side effects when high drug concentrations in the circulation are required to elicit a therapeutic response in the CV tract (5). To reduce side effects and achieve localized therapy, recent efforts have increasingly emphasized topical drug delivery methods, such as creams, hydrogels, and inserted devices, to deliver therapeutics to the apical side of the cervix epithelium (6–11). Apical drug delivery may also be extended to protection against sexual transmission of infections, because neutralizing antibodies and microbicides must act at mucosal surfaces to block the entry of pathogens (12–15).

Nanoparticle systems possess desirable features for treatment, including: (*i*) sustained and controlled release of drugs locally (16), (*ii*) potential to cross the mucosal barrier due to the nanometric size (17–19), (*iii*) rapid intracellular trafficking to the perinuclear region of underlying cells (20), and (*iv*) protection of cargo therapeutics from degradation and removal in the mucus (21, 22). However, therapeutic and/or diagnostic particles must overcome the mucosal barrier lining the CV tract to reach underlying cells and avoid clearance. Mucins, highly glycosylated large proteins (10–40 MDa) secreted by epithelial cells, represent the principal component of the entangled viscoelastic gel that protects the underlying epithelia from entry of pathogens and toxins (23–26). Other mucus constituents, such as lipids, salts, macromolecules, cellular debris, and water, work together with mucins to form a nanoscopically heterogeneous environment for nanoparticle transport, where the shear-dependent bulk viscosity is typically 100–10,000 times more viscous than water (24). Small viruses up to 55 nm have been shown to diffuse in CV mucus as rapidly as in water; however, a larger virus, 180-nm herpes simplex virus, was slowed 100- to 1,000-fold by CV mucus compared with water, suggesting that the mucus mesh spacing is ≈20–200 nm (27, 28). It was also previously reported that polystyrene particles (59–1,000 nm) adhered tightly to cervical mucus, rendering them completely immobile (27). These observations have suggested that the transport of synthetic polymer nanoparticles, especially those larger than ≈59 nm, was unlikely to occur efficiently enough to allow access of sustained release particles to underlying epithelium in human mucus-covered tissues.

To investigate and potentially improve the transport of nanoparticles across the CV mucus barrier, we studied the quantitative transport rates of hundreds of individual nanoparticles of various sizes and surface chemistries in human CV secretions. Undiluted mucus at physiologically relevant conditions was obtained by a recently described procedure that uses a menstrual-collection device (29). Surprisingly, we report that nanoparticles larger than the previously reported CV mucus mesh spacing are capable of rapid transport in CV mucus if they are coated with the mucoresistant polymer, low-molecular-weight polyethylene glycol.

## Results

**Real-Time Transport of COOH-Modified Nanoparticles.** We first sought to determine the effect of particle size on transport rates in CV mucus obtained from human volunteers. The hydrodynamic diameters of the particles suspended in water, characterized by dynamic light scattering, are listed in Table 1. The addition of uncoated particle at relatively high concentration (2% particles by weight) to CV mucus caused collapse of the mucus fibers into bundles that trapped the particles and pre-

Author contributions: S.K.L., R.C., and J.H. designed research; S.K.L., D.E.O., S.H., S.T.M., and Y.-Y.W. performed research; S.K.L., D.E.O., S.H., S.T.M., and Y.-Y.W. analyzed data; and S.K.L., R.C., and J.H. wrote the paper.

The authors declare no conflict of interest.

This article is a PNAS direct submission.

Abbreviations: COOH-PS, COOH-modified particles; CV, cervicovaginal; $D_{eff}$, effective diffusivity; MSD, mean-squared displacements; PEG-PS, PEGylated particles; RC, relative change.

‖To whom correspondence should be addressed. E-mail: hanes@jhu.edu.

This article contains supporting information online at www.pnas.org/cgi/content/full/0608611104/DC1.

**Table 1. Characterization of COOH- and PEG-modified nanoparticles and ratios of the ensemble average diffusion coefficients in cervicovaginal mucus ($D_m$) compared to water ($D_w$)**

| Size, nm* | Surface chemistry | Diameter, nm | ζ-potential, mV | Avidin adsorption, %† | $D_m/D_w$‡ |
|---|---|---|---|---|---|
| 100 | COOH | 109.2 ± 3.1 | −41.0 ± 1.9 | 97.6 | 2.3 E −5 |
| 100 | PEG | 122.4 ± 5.2 | −4.4 ± 1.1 | 2.9 | 4.6 E −4 |
| 200 | COOH | 216.6 ± 4.5 | −58.8 ± 4.2 | 99.1 | 4.2 E −4 |
| 200 | PEG | 232.3 ± 6.8 | −2.1 ± 0.3 | 2.8 | 1.6 E −1 |
| 500 | COOH | 515.0 ± 7.2 | −61.0 ± 0.5 | 100.0 | 2.2 E −4 |
| 500 | PEG | 529.1 ± 8.1 | −5.6 ± 0.4 | 3.1 | 2.5 E −1 |

*Provided by the manufacturer.
†Adsorption of avidin calculated based on average maximum fluorescence intensity.
‡Effective diffusivity values are calculated at a time scale of 1 s. $D_w$ is calculated from the Stokes–Einstein equation.

vented their transport (data not shown). However, low concentration of particles (0.008% particles by weight) did not cause bundling and allowed particle movement [supporting information (SI) Movie 1]. Surprisingly, 200- and 500-nm COOH-modified particles (COOH-PS) displayed higher transport rates, as measured by geometric ensemble mean-squared displacements (<MSD>), than otherwise similar 100-nm particles (Fig. 1*A*). At a time scale of 1 s, 100-nm COOH-PS particles were 9- and 2-fold slower than 200- and 500-nm COOH-PS particles, respectively. The ensemble-average effective diffusivity ($<D_{eff}>$) of COOH-PS particles decreases at short time scales (Fig. 1*B*), as expected in mucus (17). By fitting particle MSD vs. time scale ($\tau$) to the equation $MSD = 4D_o\tau^{\alpha}$, where $D_o$ is the diffusion coefficient independent of time scale, one can obtain an average value for $\alpha$ that provides insight into the extent of impediment to particle motion ($\alpha = 1$ for pure unobstructed Brownian diffusion, such as particles in water). Average $\alpha$ values were 0.16, 0.36, and 0.43 for 100-, 200-, and 500-nm COOH-PS particles, respectively. Overall, the ensemble-average $D_{eff}$ of 100-, 200-, and 500-nm COOH-PS particles in mucus (at $\tau = 1$ s) were reduced by 44,000-, 590-, and 4,600-fold compared with the same particles in water (Table 1).

To begin to understand the mechanistic reasons for the unexpectedly low mobility of 100-nm COOH-PS particles (compared with 200 and 500 nm) across all time scales, we sorted particles based on their calculated $D_{eff}$ (at $\tau = 1$ s) into 10 groups (Fig. 1*C*). Although the fastest 10% of 100-nm COOH-PS particles had approximately similar mean $D_{eff}$ as compared with 200- and 500-nm COOH-PS particles, the mean $D_{eff}$ values for 200- and 500-nm COOH-PS particles were greater than for 100-nm COOH-PS particles for all other subgroups (i.e., the slowest 90% of particles), which accounts for the slower ensemble mobility of 100-nm COOH-PS particles. The $D_{eff}$ of individual particles of all sizes spanned a wide range, with the fastest and slowest particles within each particle size differing by at least 4 orders of magnitude (Fig. 1*C*). The considerable heterogeneity in $D_{eff}$ within each group of particles suggested that different mechanisms of particle transport exist. This hypothesis is supported by visual observations of both immobile and rapidly moving particles in the same movie (SI Movie 1).

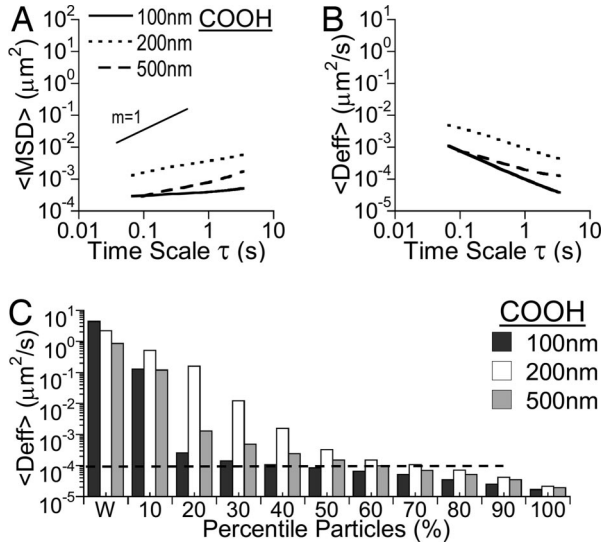


**Fig. 1.** Transport rates of COOH-modified polystyrene particles in CV mucus. (*A*) Ensemble-averaged geometric mean square displacements (<MSD>) as a function of time scale. (*B*) Effective diffusivities ($<D_{eff}>$) as a function of time scale. (*C*) Comparison of average $D_{eff}$ at a time scale of 1 s in water (W) vs. CV mucus of subfractions of particles, from fastest to slowest. Theoretical $D_{eff}$ for same sized particles in water is shown as W. The dashed black line at $<D_{eff}> = 1 \times 10^{-4}$ signifies the microscope's resolution. Data represent ensemble average of three experiments, with $n \geq 120$ particles for each experiment.

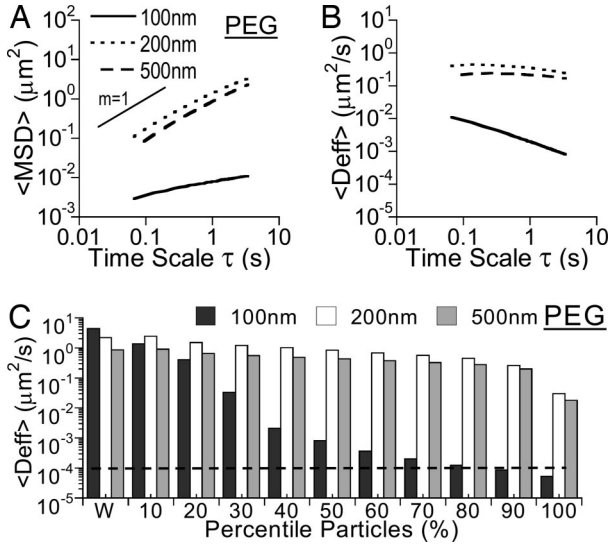


**Fig. 2.** Transport rates of PEG-modified polystyrene particles in CV mucus. (*A*) Ensemble-averaged geometric mean square displacements (<MSD>) as a function of time scale. (*B*) Effective diffusivities ($<D_{eff}>$) as a function of time scale. (*C*) Comparison of average $D_{eff}$ at a time scale of 1 s in water (W) vs. CV mucus of subfractions of particles, from fastest to slowest. Theoretical $D_{eff}$ for same sized particles in water is shown as W. The dashed black line at $<D_{eff}> = 1 \times 10^{-4}$ signifies the microscope's resolution. Data represent ensemble average of three experiments, with $n \geq 120$ particles for each experiment.

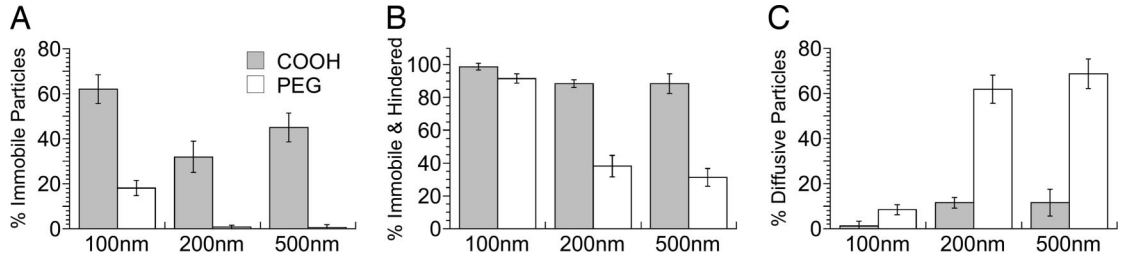


**Fig. 3.** Transport mode distributions of COOH- and PEG-modified particles in CV mucus: immobile particles (*A*), immobile and hindered particles (*B*), and diffusive particles (*C*). Data represent mean ± SD of three experiments, with $n \geq 120$ nanoparticles for each experiment. Immobile particles have an MSD below the microscope detection limit (10 nm) for entire length of video.

**Real-Time Transport of PEG-Modified Nanoparticles.** PEG, a hydrophilic and uncharged polymer, was covalently attached to the surface of 100-, 200-, and 500-nm particles in an attempt to reduce particle interactions with CV mucus. The extent of PEG attachment was comparable for all particles, as shown by their near-neutral surface charges and similar efficiencies in resisting adsorption of fluorescently labeled avidin (Table 1). PEGylation greatly increased particle transport rates, as is evident by the 20-, 400-, and 1,100-fold higher ensemble MSDs ($\tau$ = 1 s) of 100-, 200-, and 500-nm PEGylated particles (PEG-PS) compared with corresponding COOH-PS particles of the same size (Fig. 2*A* and SI Movie 2). The $<D_{eff}>$ ($\tau$ = 1 s) for 100-, 200-, and 500-nm PEG-PS were reduced by only 2,000-, 6-, and 4-fold compared with that of the expected values for their diffusion in water (Table 1). The ensemble $D_{eff}$s of PEG-PS of all three sizes still decreased with increasing time scale (Fig. 2*B*), but only 100-nm PEG-PS experienced extensive obstruction to transport ($\alpha$ = 0.31, 0.81, and 0.89 for 100-, 200-, and 500-nm PEG-PS, respectively). PEGylation not only reduced impediment for larger PEG-PS (200 and 500 nm) but also increased the homogeneity of transport compared with similar-sized COOH-PS particles (Fig. 2*C*).

**Analysis of Transport Mechanisms.** For all sizes studied, a large fraction of COOH-PS particles appeared to be immobilized by adhering extensively to CV mucus, resulting in an MSD below the resolution of the microscope (SI Fig. 5*A*). A significant percentage of the remaining COOH-PS particles underwent hindered diffusive motions or transport that is restricted by obstacles in the fluid microenvironment (SI Fig. 5*B*). Consequently, only a small fraction of COOH-PS particles exhibited Brownian or near-Brownian trajectories (SI Fig. 5*C*), whereas such trajectories were evident for a large fraction of 200- and 500-nm PEG-PS. Therefore, to further understand the unexpected rapid transport of large PEG-PS and to explain the mechanism of the contribution of PEG to improved transport, we determined the percentage of particles undergoing specific modes of transport (diffusive, hindered-diffusive, or immobile).

The greatly improved transport rates upon PEGylation, especially for larger particles, were largely due to a marked reduction in the number of immobile particles in CV mucus across all particle sizes tested (Fig. 3*A*). Nearly 20% of 100-nm PEG-PS were immobile, but <0.5% of 200- and 500-nm PEG-PS were immobile. In general, PEG led to an increased number of particles with greater mobility, as seen by a large shift in the transport modes from immobile to hindered-diffusion and from hindered-diffusion to diffusive (Fig. 3*B*). Within the size range studied here, PEGylation increased the fraction of diffusive particles between 5- and 7-fold (Fig. 3*C*). There was also a statistically significant increase in the percentage of diffusive particles when the particle size was increased from 100 to 200 or 500 nm (Fig. 3*C*). The difference in the percentage of hindered and diffusive particles between 200- and 500-nm samples was not statistically significant (Fig. 3, $P > 0.05$) for both surface chemistries tested. Furthermore, PEGylation also improved the overall transport rates of similar-sized particles undergoing hindered transport for all particle sizes (SI Fig. 6). At a time scale of 1 s, PEGylated particles displayed 6.0-, 99-, and 140-fold faster transport within the hindered diffusion regime than their non-PEGylated 100-, 200-, and 500-nm counterparts, respectively.

Within the hindered populations, 200-nm PEG-modified particles displayed the greatest mobility, and even 500-nm PEGylated particles moved much more rapidly than similar 100-nm particles (SI Fig. 6). However, considering exclusively the diffusive population of particles, an increase in particle size reduced transport rates, and 100-nm particles exhibited the fastest transport rates for both COOH- and PEG-modified surfaces, as expected (SI Fig. 7). For diffusive PEGylated particles, a reduction in size from 500 to 200 or 100 nm increased the mean $D_{eff}$ by 2.3- and 3.2-fold, respectively, in adequate agreement with Stokean principles that predict 2.5- and 5-fold improvements.

**Viscosity of Human CV Mucus.** CV mucus exhibits viscosity within the range (in the higher end) of typical human mucus secretions (Fig. 4).

## Discussion

Encapsulation of drugs and genes in nanoparticles offers the potential for direct and sustained delivery to the underlying epithelial cells in mucus-covered tissues (30, 31), including the CV tract, thus minimizing systemic toxicity and degradation of the cargo therapeutics in serum. Nanoparticles must quickly traverse CV mucus layers that are up to a few hundred microns thick to reach the underlying epithelia and avoid mucus clearance mechanisms (24). An important role of mucus barriers is to trap foreign particles and then clear them from the body before they reach the underlying epithelia (24, 31). The mucus barrier has been cited as a critical

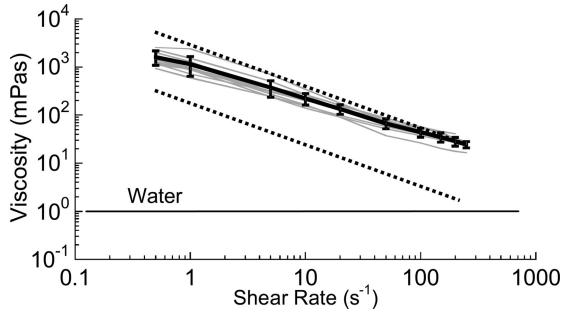


**Fig. 4.** Viscosity of fresh human CV mucus samples measured as a function of shear rate. Thin black lines represent $n$ = 13 CV mucus samples. Thick line represents the average. The estimated range of a variety of other human mucus samples, including lung, gastric, small intestine, sputum, and colon mucus is plotted (dashed lines) based on ref. 24.

bottleneck in the treatment of a variety of diseases (17, 24, 31–34), and it has been widely suggested that nanoparticles are unable to efficiently traverse mucus layers (35–39), including CV mucus (27). For applications in CV diseases, the need for improved particle transport is further underscored by: (*i*) the previous observation that polystyrene beads firmly adhere to mucin fibers in human CV secretions, rendering them completely immobile (27); (*ii*) there is 100- to 1,000-fold reduced $D_{eff}$ for herpes simplex virus ($d$ = 180 nm) in CV mucus compared with water (27); and (*iii*) there are existing estimates of CV mucus mesh pore size of 10 to at most 200 nm from fluorescence recovery after photobleaching (FRAP) and most electron microscopy studies (27, 28). The prevalent dogma in the design of nanoparticle therapeutics targeted to mucosal epithelia is that large nanoparticles, preferred for higher drug-encapsulation efficiency and favorable drug-release kinetics, are not capable of crossing mucosal barriers.

Surprisingly, we report that the transport of PEG-coated polymer particles larger than the reported CV mucus-mesh size was not significantly impeded by CV mucus. Specifically, using multiple particle tracking, which traces the motions of hundreds of individual particles with high temporal and spatial resolution, we found that size, surface chemistry, and particle concentration all critically influence the transport of particles in human CV mucus. The most surprising findings were: (*i*) larger polymeric nanoparticles (up to 500 nm) with a dense polyethylene-glycol coating can diffuse through CV mucus with rates up to one-fourth as fast as they would in pure water; and (*ii*) 100-nm particles moved much more slowly through CV mucus than either 200- or 500-nm particles. The faster transport of 200- and 500-nm particles, regardless of surface chemistry (COOH or PEG), not only is contrary to the expectation that smaller particles should move faster in mucus (17, 18, 27) but also directly opposes the earlier estimates of CV mucus mesh spacing (27, 28). Greater steric hindrance from the mucin fiber network and elevated friction forces was expected, *a priori*, to result in slower transport for larger particles in CV mucus. However, we observed both greater immobile and hindered-diffusion fractions for 100-nm particles compared with either 200- or 500-nm particles for both COOH- and PEG-modified surfaces. The large fraction of 200- and 500-nm particles that underwent diffusive transport (e.g., as opposed to hindered diffusion) directly implied that the upper range of effective mesh spacing in human CV secretions must be significantly larger than earlier reports and must include a large number of pores with effective spacings substantially larger than 500 nm. This spacing is consistent with the only electron microscopic investigation in which the mucus gel was prepared by freeze substitution (40). With this method, the spacing between the primary fibrous elements was 500–800 nm, suggesting freeze substitution may cause minimal disturbance of the native distribution of mucin fibers.

The rapid mucosal transport of 200- and 500-nm PEG-modified particles has important implications for the development of therapeutic and imaging applications *in vivo*. Larger nanoparticles afford substantially higher drug encapsulation efficiency, and the release of drugs from small nanoparticles (<100–200 nm) is difficult to control. The high surface-area-to-volume ratio of small nanoparticles typically leads to fast diffusion of drugs out of particles (i.e., the burst effect) within hours upon *in vitro* or *in vivo* application (41, 42). As the size of drug-loaded particles increases, drug-release kinetics are usually greatly improved, and sustained release of therapeutics over days and even months can be achieved with enhanced therapeutic efficacies (30, 43, 44).

It is possible that large PEGylated nanoparticles may also transport quickly in mucus coating other entry sites into the body. Mucus coatings of the CV tract, airways of the lungs, gastrointestinal tract, nose, eyes, and epididymus all have similar components, and all possess similar rheological properties (Fig. 4). In particular, the mucin glycoform MUC5B has been identified as the major secreted form of mucin in the mucosal layers protecting the CV tract (45, 46), lungs (46, 47), nose (48), and eye (49). The mucin content, ≈1–3% by weight, is also similar among cervical, nasal, and lung mucus (50–54). The composition of water in the aforementioned mucus types all falls within the range of 90–98% (52, 53, 55–57). The similar mucus composition and mucin glycoforms leads to similar rheology, characterized by log-linear shear thinning of viscosity. It should be recognized, however, that, with the exception of mucus expectorated by patients with cystic fibrosis, it remains very difficult to obtain fresh undiluted human mucus from sites other than the CV tract.

The transport of hydrophobic polystyrene particles without PEG modification was characterized by significant entrapment within and adhesion to the mucosal network, presumably because of the hydrophobic polystyrene bead-forming polyvalent bonds with hydrophobic domains distributed along mucin fibers (27, 35). However, it was not obvious, *a priori*, that PEG may reduce association of particles with mucus components, because high-molecular mass PEG (>10 kDa) has been shown to exhibit mucoadhesive properties involving interpenetration of the polymer with mucus fibers (58). Looking to nature for guidance, we noted that viruses capable of rapid transport in mucus possess surfaces that are densely coated equally with positive and negative charges, creating a hydrophilic and net-neutral shell that minimizes hydrophobic and electrostatic adhesive interactions (24). However, the engineering of densely charged (average distance between charges, ≈5 Å) yet neutral surfaces on synthetic particles is exceedingly difficult. We hypothesized that coating particles with PEG, an uncharged hydrophilic polymer routinely used in pharmaceutics, may reduce particle–mucus adhesive interactions if the molecular mass of PEG was too low to support adhesion by polymer interpenetration. We show here that, contrary to reports of PEG as mucoadhesive, coating particles with 2-kDa PEG chains led to a greatly increased percentage of diffusive particles and up to 3 orders of magnitude faster transport.

It is unlikely that the rapid transport of PEGylated particles is due to alterations of the mucus structure, because they do not interact significantly with mucus. Instead, particles likely move in low-viscosity channels or pores within the mucus, as suggested in our earlier work on particle transport in cystic fibrosis mucus (17). We have recently found that PEGylated particles move much faster in cystic fibrosis mucus than non-PEGylated particles of equal size over time scales of at least 40 min and distances of at least 7.4 $\mu$m using biodegradable poly(ether-anhydride) nanoparticles [our unpublished results; the polymer has been described (59)], suggesting that transport rates of PEGylated particles measured at short time scales correlate well with those measured at long time scales in mucus.

One possible explanation for the significant fraction of 100-nm PEG-modified particles that remain immobile in the mucosal network (whereas <0.5% of 200- and 500-nm PEG-PS are immobile) may be attributed to inadequate PEGylation of 100-nm (vs. 200- or 500-nm) particles. Smaller particles, because of a greater degree of curvature, may require higher surface density of hydrophilic PEG molecules to sufficiently shield the hydrophobic core. However, the effectiveness of the PEG shield, as measured by surface charge and resistance to avidin adsorption, appeared similar for all particles studied. Alternatively, the unexpected slower transport of 100-nm particles in the viscoelastic CV mucus gel may be partially explained by principles from size-exclusion chromatography. According to this theory, for particles of various sizes traveling in a network with heterogeneous pore sizes, smaller particles can access a greater number of small pores or pockets in the gel, resulting in an overall reduced transport rate over long distances because of the greatly increased tortuosity of their average path. Larger particles that are unable to diffuse into small pores move instead in less-restricted low-viscosity channels, with much larger mesh spacing.

It seems unlikely, however, that this hypothesis can be reconciled with the previous observation that viruses <55 nm in diameter can diffuse basically unhindered in CV mucus (27). We were able to rule out aggregation as a potential explanation for the slower transport of 100-nm particles for several reasons: (*i*) particles were not aggregated before addition to mucus (or glycerol; results not shown), as measured by dynamic light scattering; (*ii*) high particle monodispersity was observed in both glycerol and mucus, where polydispersity is expected for aggregated particles; (*iii*) we found that measured transport rates of particles in glycerol correctly reflect its viscosity based on the Stokes–Einstein equation; and (*iv*) heavily PEGylated nanoparticles are highly resistant to aggregation.

A number of reports have examined particle size and transport or cellular uptake in mucosal environments; however, none has reported observations of smaller particles moving more slowly than larger particles (35–39). The majority of studies compared particle sizes spanning orders of magnitude and concluded that smaller particles move faster (36–38). It is difficult to directly compare these studies to the results reported here, given the large deviation in the range of particle sizes previously studied and the different types of mucus tested. Others have reported that permeability values decreased sharply as the particle size was increased from 100 to 300 nm in synthetic gastric mucin gels or rat gastrointestinal mucosa (35, 39). It remains unknown whether the discrepancy between these findings and ours is a consequence of differences in the biophysical structure of the mucin fiber networks (i.e., synthetic formulations vs. physiological secretions), the types of mucus being compared, and/or collection and handling methods used.

Differences between our study and the previous report by Cone and coworkers (27) led us to another important finding. Specifically, we found that a significant number of polystyrene particles were able to move in human cervical mucus, whereas Olmsted *et al.* reported that all particles were immobile (27). The principal differences between the two studies may be related to the concentration of particles used. The experiments performed here used diluted COOH-PS and PEG-PS, whereas the Olmsted study used more concentrated COOH-PS. We found that the addition of high concentrations of COOH-PS particles collapsed mucus fibers into bundles (data not shown) in a manner similar to that observed in the Olmsted study. In the latter case, the concentrated particle solution likely contains a sufficient number of particles to impart a hydrophobic force capable of affecting the mucosal network structure. Once the mucin fibers collapse around the particles, there are sufficient hydrophobic interactions to stabilize the particles, resulting in complete retardation of transport. The observation that the concentration of particles may critically affect the transport in mucus warrants further study. By eliminating the hydrophobic interactions between mucin fibers and hydrophobic polystyrene core, PEGylation may allow delivery of rapidly moving particles to the mucosa at higher concentrations than otherwise possible with uncoated particles, potentially increasing the concentration of therapeutics that can be delivered to the mucosal surfaces of the body.

## Summary

Unexpectedly, large (200- to 500-nm) particles transport much more rapidly than 100-nm particles in human CV mucus. This finding should strongly encourage the commercial development of new nanoparticle-based drug delivery systems for the CV tract and potentially other mucosal surfaces, because drug-delivery kinetics and loading efficiency are vastly improved as particle diameter increases. Our study also suggests that a larger effective mucus-mesh size exists for CV mucus than previously reported. Particle concentration may also play an important role in particle transport across mucosal barriers and, therefore, should be studied further. The design of particles with improved physical (e.g., size) and chemical (e.g., surface chemistry) properties may lead to improved drug delivery to the CV tract by enhancing the ability of drug-delivery systems to cross the mucus barrier.

## Materials and Methods

**CV Mucus Collection and Preparation.** The CV mucus-collection procedure was performed as published (29); details are provided in *SI Text*. Collected mucus was used for microscopy within 4 h. The viscosity of fresh samples was observed as a function of shear rate at 37°C in a Brookfield cone and plate viscometer (Model HADV-III with CP-40 spindle; Brookfield, Middleboro, MA).

**Nanoparticle Preparation and Characterization.** One hundred- to 500-nm yellow-green fluorescent carboxyl-modified polystyrene particles (Molecular Probes, Eugene, OR) were covalently modified with diamine PEG (molecular mass, ≈2 kDa; Nektar Therapeutics, San Carlos, CA) by carboxyl-amine reaction in 3:1 excess, following manufacturer-suggested protocol, as published (60); details are provided in *SI Text*. Size and ξ-potential were determined by dynamic light scattering and laser Doppler anemometry, respectively, using a Zetasizer 3000 (Malvern Instruments, Southborough, MA). Size measurements were performed at 25°C at a scattering angle of 90°. Samples were diluted in double-distilled water and measurements performed according to instrument instructions.

**Protein Adsorption to Particles and Measure of PEGylation Effectiveness.** To confirm PEG attachment and quantify efficiency in resisting protein adsorption by PEG, 10 μl of COOH particles and PEG-modified particles (≈0.04% by mass) were added to 200 μl of 0.1 mg/ml rhodamine fluorescent NeutrAvidin (Molecular Probes) and incubated on an orbital shaker for 1 h. Particles were subsequently washed twice in PBS, resuspended to a final concentration of 0.008% by mass, and observed on sealed glass slides or coverslips by using a confocal microscope [Zeiss (Thornwood, NY) LSM 510] equipped with a 100×/1.4-N.A. oil-immersion lens (SI Fig. 8). Samples were excited with 488 and 543 lasers, and the pinhole was adjusted to obtain optical slices ranging from <0.7 to 0.8 μm. Identical excitation and detection settings were maintained, and all samples were tested sequentially. Particles without avidin incubation served as negative control to ensure negligible bleach over. Maximum pixel intensity for each particle, after conversion to gray scale, was analyzed by using SCION Image 4.03b (Scion Corp., Frederick, MD).

**Multiple Particle Tracking in CV Mucus.** Particle transport rates were measured by analyzing trajectories of fluorescent particles, recorded by using a silicon-intensified target camera (VE-1000, Dage-MTI, Michigan, IN) mounted on an inverted epifluorescence microscope equipped with 100× oil-immersion objective (N.A., 1.3). Experiments were carried out in 8-well glass chambers (LabTek, Campbell, CA), where diluted particle solutions (0.0082% wt/vol) were added to 250–500 μl of fresh mucus to a final concentration of 3% vol/vol (final particle concentration, $8.25 \times 10^{-7}$ wt/vol) and incubated for 2 h before microscopy. Trajectories of $n > 120$ particles were analyzed for each experiment, and three experiments were performed for each condition. Movies were captured with Metamorph software (Universal Imaging, Glendale, WI) at a temporal resolution of 66.7 ms for 20 s. The tracking resolution was 10 nm, determined by tracking displacements of particles immobilized with a strong adhesive (61). The coordinates of nanoparticle centroids were transformed into time-averaged MSD, $\langle \Delta r^2(\tau) \rangle = [x(t+\tau) - x(t)]^2 + [y(t+\tau) - y(t)]^2$ ($\tau$ = time scale or time lag), from which distributions of MSDs and effective diffusivities were calculated, as demonstrated (17, 62, 63). Additional information for measuring 3D transport by 2D particle tracking is provided in *SI Text* and in a recent review (21).

**Particle Transport-Mode Classification.** The mechanism of particle transport over short and long time scales was classified based on the concept of relative change (RC) of $D_{eff}$, as discussed (60, 64). In brief, RC values of particles at short and long time scales were calculated by dividing the $D_{eff}$ of a particle at a probed time scale by the $D_{eff}$ at an earlier reference time scale. By calculating RC values for two time regimes (i.e., short and long time scales), one can obtain the transport mode that describes the particle transport properties over different length and temporal scales. $RC_{short}$ was defined at $\tau_{ref} = 0.2$ s, and $\tau_{probe} = 1$ s, whereas $RC_{long}$ was found at reference $\tau_{ref} = 1$ s and $\tau_{probe} = 2$ s. The rigor of the transport-mode classification was confirmed by the slopes of the MSD vs. time-scale plots, where diffusive particles possess a slope of $\approx 1$, and where the slope for hindered particles progressively decrease from 1 with increasing time scale (SI Figs. 6 and 7). Additional details are provided in *SI Text*.

We thank Kok Leong Choy and Yoojin An for assistance in PEGylation and Vikash Chauhan for insightful discussion. We also express our gratitude for support from the Integrated Imaging Center (IIC, Johns Hopkins University), especially Ned Perkins and the IIC director, Michael McCaffery. We gratefully acknowledge support for S.K.L. from the Natural Science and Engineering Research Council of Canada.

1. Thigpen T (2003) *Cancer J* 9:425–432.
2. Robinson WR, Andersen J, Darragh TM, Kendall MA, Clark R, Maiman M (2002) *Obstet Gynecol* 99:777–784.
3. Buda A, Dell'Anna T, Signorelli M, Mangioni C (2003) *Oncology* 65:63–66.
4. Duenas-Gonzalez A, Cetina L, Mariscal I, de la Garza J (2003) *Cancer Treat Rev* 29:389–399.
5. Serkies K, Jassem J (2005) *Crit Rev Oncol Hematol* 54:197–208.
6. Sherwood JK, Zeitlin L, Whaley KJ, Cone RA, Saltzman M (1996) *Nat Biotechnol* 14:468–471.
7. McCormack WM, Covino JM, Thomason JL, Eschenbach DA, Mou S, Kapernick P, McGregor J, Rein MF, Hillier SL (2001) *Sex Transm Dis* 28:569–575.
8. Shen H, Goldberg E, Saltzman WM (2003) *J Controlled Release* 86:339–348.
9. Justin-Temu M, Damian F, Kinget R, Van Den Mooter G (2004) *J Womens Health (Larchmt)* 13:834–844.
10. Hussain A, Ahsan F (2005) *J Controlled Release* 103:301–313.
11. Zeitlin L, Hoen TE, Achilles SL, Hegarty TA, Jerse AE, Kreider JW, Olmsted SS, Whaley KJ, Cone RA, Moench TR (2001) *Sex Transm Dis* 28:417–423.
12. Roden RB, Ling M, Wu TC (2004) *Hum Pathol* 35:971–982.
13. Zeitlin L, Cone RA, Whaley KJ (1999) *Emerg Infect Dis* 5:54–64.
14. Radomsky ML, Whaley KJ, Cone RA, Saltzman WM (1992) *Biol Reprod* 47:133–140.
15. Sherwood JK, Zeitlin L, Chen XL, Whaley KJ, Cone RA, Saltzman WM (1996) *Biol Reprod* 54:264–269.
16. Allen TM, Cullis PR (2004) *Science* 303:1818–1822.
17. Dawson M, Wirtz D, Hanes J (2003) *J Biol Chem* 278:50393–50401.
18. Dawson M, Krauland E, Wirtz D, Hanes J (2004) *Biotechnol Prog* 20:851–857.
19. Prego C, Garcia M, Torres D, Alonso MJ (2005) *J Controlled Release* 101:151–162.
20. Suh J, Wirtz D, Hanes J (2003) *Proc Natl Acad Sci USA* 100:3878–3882.
21. Suh J, Dawson M, Hanes J (2005) *Adv Drug Delivery Rev* 57:63–78.
22. Janes KA, Calvo P, Alonso MJ (2001) *Adv Drug Delivery Rev* 47:83–97.
23. Carlstedt I, Sheehan JK (1989) *Symp Soc Exp Biol* 43:289–316.
24. Cone R (1999) in *Mucosal Immunology*, eds Ogra PL, Mestecky J, Lamm ME, Strober W, Bienenstock J, McGhee JR (Academic, San Diego), 2nd Ed, pp 43–64.
25. Sanders NN, De Smedt SC, Demeester J (2000) *J Pharmacol Sci* 89:835–849.
26. Thornton DJ, Sheehan JK (2004) *Proc Am Thorac Soc* 1:54–61.
27. Olmsted SS, Padgett JL, Yudin AI, Whaley KJ, Moench TR, Cone RA (2001) *Biophys J* 81:1930–1937.
28. Saltzman WM, Radomsky ML, Whaley KJ, Cone RA (1994) *Biophys J* 66:508–515.
29. Boskey ER, Moench TR, Hees PS, Cone RA (2003) *Sex Transm Dis* 30:107–109.
30. Langer R (1998) *Nature* 392:5–10.
31. Hanes J, Dawson M, Har-el Y, Suh J, Fiegel J (2003) in *Pharmaceutical Inhalation Aerosol Technology*, ed Hickey AJ (Dekker, New York), pp 489–539.
32. Khanvilkar K, Donovan MD, Flanagan DR (2001) *Adv Drug Delivery Rev* 48:173–193.
33. Garcia-Contreras L, Hickey AJ (2002) *Adv Drug Delivery Rev* 54:1491–1504.
34. Sanders NN, De Smedt SC, Van Rompaey E, Simoens P, De Baets F, Demeester J (2000) *Am J Respir Crit Care Med* 162:1905–1911.
35. Norris DA, Sinko PJ (1997) *J Appl Polym Sci* 63:1481–1492.
36. Szentkuti L (1997) *J Controlled Release* 46:233–242.
37. Ron N, Thies C (1998) *Proc Controlled Rel Soc* 25:376–377.
38. Florence AT (1997) *Pharmacol Res* 14:259–266.
39. Delie F (1998) *Adv Drug Delivery Rev* 34:221–233.
40. Yudin AI, Hanson FW, Katz DF (1989) *Biol Reprod* 40:661–671.
41. Fu K, Harrell R, Zinski K, Um C, Jaklenec A, Frazier J, Lotan N, Burke P, Klibanov AM, Langer R (2003) *J Pharmacol Sci* 92:1582–1591.
42. Gref R, Minamitake Y, Peracchia MT, Trubetskoy V, Torchilin V, Langer R (1994) *Science* 263:1600–1603.
43. Kim DH, Martin DC (2006) *Biomaterials* 27:3031–3037.
44. Yoo HS, Oh JE, Lee KH, Park TG (1999) *Pharmacol Res* 16:1114–1118.
45. Gipson IK, Spurr-Michaud S, Moccia R, Zhan Q, Toribara N, Ho SB, Gargiulo AR, Hill JA, 3rd (1999) *Biol Reprod* 60:58–64.
46. Wickstrom C, Davies JR, Eriksen GV, Veerman EC, Carlstedt I (1998) *Biochem J* 334:685–693.
47. Rose MC, Nickola TJ, Voynow JA (2001) *Am J Respir Cell Mol Biol* 25:533–537.
48. Groneberg DA, Peiser C, Dinh QT, Matthias J, Eynott PR, Heppt W, Carlstedt I, Witt C, Fischer A, Chung KF (2003) *Laryngoscope* 113:520–524.
49. Davidson HJ, Kuonen VJ (2004) *Vet Ophthalmol* 7:71–77.
50. Carlstedt I, Lindgren H, Sheehan JK, Ulmsten U, Wingerup L (1983) *Biochem J* 211:13–22.
51. Chao, C-cW, Butala SM, Herp A (1988) *Exp Eye Res* 47:185–196.
52. Quraishi MS, Jones NS, Mason J (1998) *Clin Otolaryngol* 23:403–413.
53. Samet JM, Cheng PW (1994) *Environ Health Perspect* 102:89–103.
54. Allen A, Flemstrom G, Garner A, Kivilaakso E (1993) *Physiol Rev* 73:823–857.
55. Gipson IK (2001) *Front Biosci* 6:1245–1255.
56. Chao C-CW, Vergnes J-P, Brown SI (1983) *Exp Eye Res* 36:139–150.
57. Engel E, Guth PH, Nishizaki Y, Kaunitz JD (1995) *Am J Physiol* 269:G994–G999.
58. Huang Y, Leobandung W, Foss A, Peppas NA (2000) *J Controlled Release* 65:63–71.
59. Fu J, Fiegel J, Hanes J (2004) *Macromolecules* 37:7174–7180.
60. Suh J, Choy KL, Lai SK, Suk JS, Tang B, Prabhu S, Hanes J (2007) *Int J Nanomed*, in press.
61. Apgar J, Tseng Y, Fedorov E, Herwig MB, Almo SC, Wirtz D (2000) *Biophys J* 79:1095–1106.
62. Valentine MT, Perlman ZE, Gardel ML, Shin JH, Matsudaira P, Mitchison TJ, Weitz DA (2004) *Biophys J* 86:4004–4014.
63. Mason TG, Ganesan K, vanZanten JH, Wirtz D, Kuo SC (1997) *Phys Rev Lett* 79:3282–3285.
64. Suk JS, Suh J, Lai SK, Hanes J (2007) *Exp Biol Med*, in press.